Chinese Chemical Letters 36 (2025) 110023

Contents lists available at ScienceDirect

Chinese Chemical Letters

journal homepage: www.elsevier.com/locate/cclet

Multidimensional detection of roxarsone *via* AIE-based sulfates

Haibo Wan[a,1], Zhengzhong Lv[b,1], Jicai Jiang[a], Xuefeng Cheng[a], Qingfeng Xu[a,*], Haibin Shi[b,*], Jianmei Lu[a,*]

[a] College of Chemistry, Chemical Engineering and Materials Science, Collaborative Innovation Center of Suzhou Nano Science and Technology, Soochow University, Suzhou 215123, China

[b] State Key Laboratory of Radiation Medicine and Protection, School for Radiological and Interdisciplinary Sciences (RAD-X) and Collaborative Innovation Center of Radiation Medicine of Jiangsu Higher Education Institutions, Soochow University, Suzhou 215123, China

ARTICLE INFO

Article history:
Received 15 March 2024
Revised 14 May 2024
Accepted 16 May 2024
Available online 18 May 2024

Keywords:
Aggregation-induced emission
SuFEx
ROX
Fluorescent detection
Living cells

ABSTRACT

Improper abuse of roxarsone (ROX) in industrial production leads to harmful effects on water, soil, food, and living creatures. It is significant to detect its concentration in the environment and biosystem. Herein, two aggregation-induced emission (AIE)-active fluorescence probes, TPE-TPE and TPE-TPE-CN, are successfully synthesized *via* a sulfur(VI) fluoride exchange (SuFEx) click reaction and first employed to detect ROX in the environment and living 3T3 cells. These two probes can selectively detect ROX in water due to the synergistic effect of photoinduced electron transfer (PET) and fluorescence resonance energy transfer (FRET) between the probes and ROX. The detection limit of TPE-TPE and TPE-TPE-CN is 0.154 and 0.385 μmol/L, respectively, much lower than the safety concentration stipulated by the World Health Organization (WHO). In addition, with the aid of a color discrimination application in a smartphone, these two probes can also detect ROX in real samples (such as water, soil, and cabbage), demonstrating their excellent potential for monitoring ROX in a practical environment.

© 2025 Published by Elsevier B.V. on behalf of Chinese Chemical Society and Institute of Materia Medica, Chinese Academy of Medical Sciences.

Roxarsone (ROX), as a typical organic arsenic compound, has been widely and increasingly used in feed additives due to its low price, high antibacterial properties, and growth promotion [1,2]. However, improper usage usually results in its leakage into the environment including water, soil, food, and so on, which causes not only acute toxicity to living creatures but also the transformation into more toxic inorganic arsenic anionics, thereby giving rise to more harmful effect to the ecology [3,4]. Therefore, it is urgent to develop an efficient method to monitor its concentration in the environment.

Recently, there are numerous methods such as inductively coupled plasma-mass spectrometry (ICP-MS) [5], gas chromatography (GC) [6], and high-performance liquid chromatography (HPLC) [7] have been employed to detect ROX in water. Nevertheless, these methods usually require sophisticated machines, tedious operations, and harsh application conditions, which hinders their large-scale application. Interestingly, the fluorescence sensing method has received significant attention due to its simple operation, fast response, and high selectivity [8,9]. Nowadays, based on the interactions between the hydroxyl and nitro group in ROX and chromophores in fluorescence probes, many fluorescence probes including covalent organic framework (COF) [10], metal-organic framework (MOFs) [11–14], coordination complex [15–17] and molecularly imprinted polymer [18] have been constructed. However, the preparation of these probes usually requires strict conditions (such as high temperature and pressure) and complicated operations (such as oxygen and water-free). Additionally, the reported fluorescence probes mainly focused on ROX detection in water, there are lack of explorations of multidimensional detection in the environment (such as real water samples, soil, and food). Moreover, traditional fluorescence probes usually display aggregation-caused quenching (ACQ) effect in their solid and aggregated state, which is not conducive to water environment-based fluorescence detection [19,20]. Thus, developing a new type of fluorescence probe with easy preparation, strong emission, and multifunctional detection performance is urgently demanded.

Aggregation-induced emission (AIE)-active fluorescence probes, which exhibit strong emission in solid and aggregated states, have provided a new solution to the ACQ effect and played an influential role in pollutant sensing [21–31]. At present, there are many methods to construct AIE-active fluorescence probes, and click reaction is widely employed due to its moderate reaction condition, rapid reaction speed, and high stereoselectivity [32]. Nevertheless,

* Corresponding authors.
E-mail addresses: xuqingfeng@suda.edu.cn (Q. Xu), hbshi@suda.edu.cn (H. Shi), lujm@suda.edu.cn (J. Lu).
[1] These authors contributed equally to this work.

https://doi.org/10.1016/j.cclet.2024.110023
1001-8417/© 2025 Published by Elsevier B.V. on behalf of Chinese Chemical Society and Institute of Materia Medica, Chinese Academy of Medical Sciences.

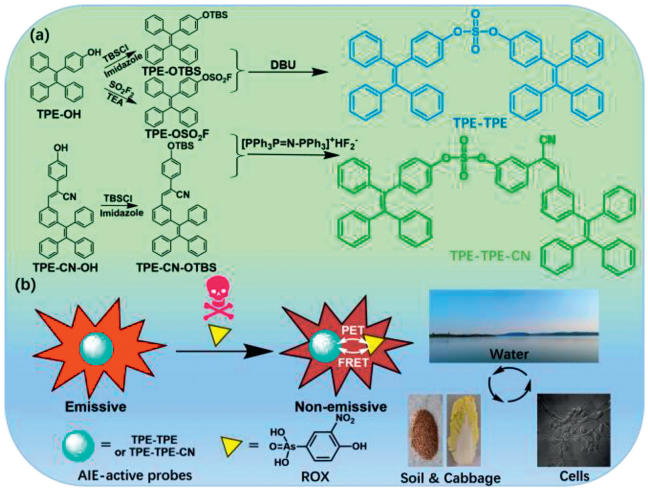

Scheme 1. (a) Synthetic routine of TPE-TPE and TPE-TPE-CN. (b) TPE-TPE and TPE-TPE-CN for multidimensional detection of ROX in water, soil, cabbage, and living cells.

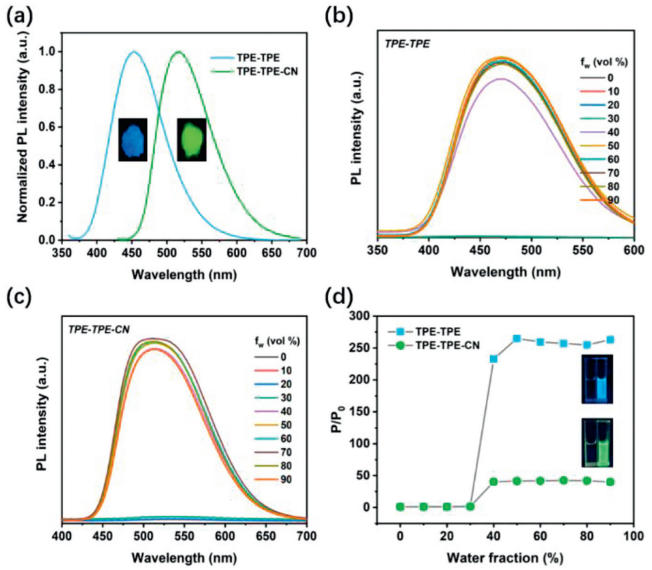

Fig. 1. (a) Solid fluorescent spectra of TPE-TPE and TPE-TPE-CN, excitation wavelength: TPE-TPE 350 nm, TPE-TPE-CN 420 nm. Inset: optical pictures of TPE-TPE and TPE-TPE-CN in solid state under UV light at 365 nm, from left to right. PL spectra of (b) TPE-TPE and (c) TPE-TPE-CN in DMF/water mixture with different water fractions (f_w, 0–90%). (d) PL intensity changes at a maximum emission wavelength of TPE-TPE and TPE-TPE-CN in different water fractions of DMF/water solution. Concentration: 20 μmol/L. Excitation wavelength: TPE-TPE 310 nm, TPE-TPE-CN 365 nm. Inset (from top to bottom): optical pictures of TPE-TPE and TPE-TPE-CN in pure DMF (left) and in DMF/water solution with 90% water fraction (right) under UV light at 365 nm. P_0 and P are the PL intensity at λ_{em} of TPE-TPE and TPE-TPE-CN in pure DMF and DMF/water solutions, respectively.

noble or transition metal salts are usually utilized in conventional click reactions, which are difficult to remove and environment-unfriendly, hindering their further application [33,34]. Interestingly, sulfur(VI) fluoride exchange (SuFEx), as a new type of click reaction with metal-free and simple postprocessing [35,36], has been employed in syntheses and modification of functional polymers [37,38], environmental treatment [39,40], electrostatic energy and memory materials [41–43], fluorescence sensing [44,45] and biomedicine [46,47]. Using SuFEx reaction, AIE-active probes with polar sulfate bonds (-OSO_2O-) can be easily obtained in the presence of a catalyst without complicated post-treatment operations, exhibiting excellent protentional in large-scale applications. However, at present, reports concerning AIE-active fluorescence probes using SuFEx reaction mainly focused on polymers and small molecular sulfate-based probes have not been reported. To the best of our acknowledge, there are no AIE-active probes for ROX detection both in the environment and living cells. In terms of the excellent fluorescence properties of AIE molecules and the high efficiency of the SuFEx reaction, it is necessary and promising to design and synthesize AIE-active sulfate fluorescence probes for multidimensional ROX detection.

In this study, two tetraphenyl ethylene derivatives with different fluorescence emissions were successfully fabricated through the SuFEx reaction at room temperature (Scheme 1). Fluorescent measurement demonstrated that these two probes exhibit AIE characteristics both in solid and aggregated states. Additionally, these two probes can be used to selectively detect ROX in water with lower detection limits. Density functional theory (DFT) calculation and spectroscopic tests confirmed that the superior detection of the probes can be ascribed to the synergistic effect of photoinduced electron transfer (PET) and fluorescence resonance energy transfer (FRET) between the probes and ROX. Moreover, these two probes can detect ROX not only in real environments (such as water, soil, and cabbage) but also in living cells, demonstrating their excellent potential in practical application.

As we all know that tetraphenyl ethylene (TPE) is a typical AIE-active chromophore [48]. Therefore, the aggregation behavior of TPE-TPE and TPE-TPE-CN in solid state and *N*,*N*-dimethylformamide (DMF)/water mixture with different water fractions (f_w) is studied, respectively. As shown in Fig. 1a, TPE-TPE powder exhibits strong blue light emission with a maximum emission wavelength (λ_{em}) of 452 nm under ultraviolet (UV) light at 365 nm, while TPE-TPE-CN strong green light emission with a λ_{em} of 516 nm in its solid state under the UV light. Furthermore, the fluorescent quantum yield (Φ_F) values of TPE-TPE and TPE-TPE-CN in solid are 16.96% and 63.19%, respectively. In solution, the photoluminescence (PL) intensity of TPE-TPE at 471 nm is low with a very weak blue-light emission and a Φ_F value of 16.26% in pure DMF (Table S1 in Supporting information). With the increase of water (f_w < 40%), its PL intensity at 471 nm shows little change. But when more water was added (f_w > 40%), the PL intensity was drastically increased and even up to 263.07-fold with a bright blue light emission and a Φ_F value of 66.11% in 90% water/DMF mixture (Figs. 1b and d). Moreover, according to the UV–visible (UV–vis) absorbance spectrum of TPE-TPE, a level-off tail effect can also be observed between 400 nm and 500 nm when f_w > 40% due to the gradual formation of organic nanoparticles (Fig. S1a in Supporting information). While its PL intensity at λ_{em} exhibits little decrease when more water is added (60% < f_w <90%) due to the strong interaction between the polar solution and the nanoparticles. Scanning electron microscope (SEM) and dynamic light scattering (DLS) analysis show that the average diameter of nanoparticles is 183.70 nm with a narrow distribution of 0.184 (Figs. S2a and b in Supporting information). Similarly, the PL intensity of TPE-TPE-CN at 514 nm is also weak with a Φ_F value of 9.50% in pure DMF, but with the increase of water fraction in DMF/water mixture (f_w < 40%), its PL intensity is gradually enhanced to 1.51-fold its original state. However, when more water was added (f_w > 40%), the PL intensity at 514 nm drastically increased to 40.25-fold its original state and remained stable around 41-fold with a Φ_F value of 61.30% in 90% water/DMF solution, and a level-off tail can also be obtained in its UV–vis absorbance spectrum, which can also be put down to the gradual formation of nanoparticles (Figs. 1c, d and Fig. S1b in Supporting information). The average diameter of nanoparticles is 207.20 nm and the polydispersity index (PDI) is 0.235, suggesting the formation of nanoparticles in 90% water/DMF solution (Figs. S2c and d in Supporting information). Moreover, the morphology

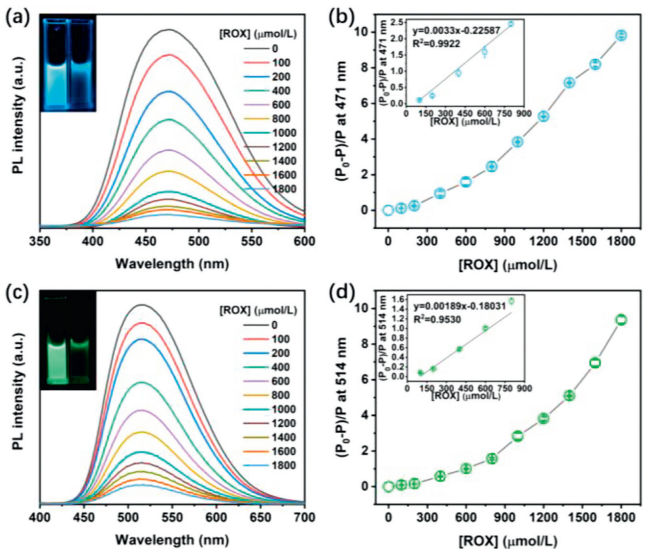

Fig. 2. PL spectrum change and a titration curve of (a, b) TPE-TPE and (c, d) TPE-TPE-CN towards ROX with different concentrations (0–1800 μmol/L) in 90% water/DMF solution. P_0 and P are the PL intensity of the probes at λ_{em} before and after addition of ROX with different concentrations in 90% water/DMF solution. Concentration: 20 μmol/L. Excitation wavelength: TPE-TPE 310 nm, TPE-TPE-CN 365 nm. Inset: optical pictures of TPE-TPE and TPE-TPE-CN before and after the addition of 1800 μmol/L of ROX under UV light at 365 nm, from left to right. Data are presented as mean ± standard deviation (SD) ($n = 3$).

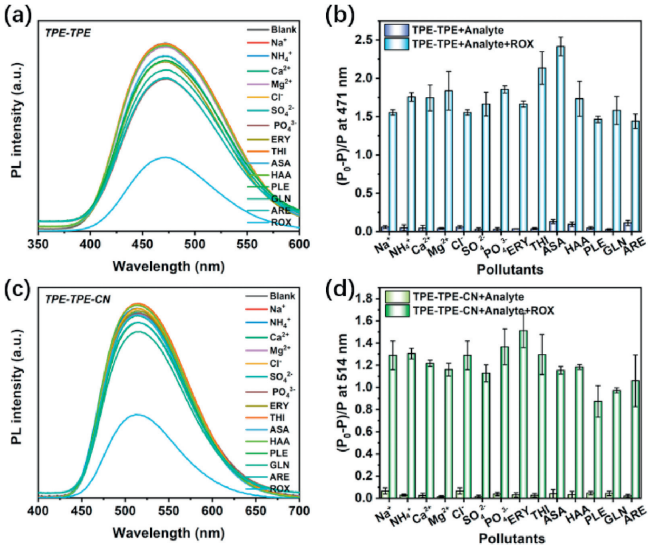

Fig. 3. Selectivity and anti-interference behaviors of TPE-TPE and TPE-TPE-CN towards ROX and other pollutants. PL spectrum changes and PL intensity changes at λ_{em} of the fluorescent probes for different pollutants with a concentration of 600 μmol/L in 90% water/DMF solution. P_0 and P are the PL intensity of the probes at λ_{em} in the absence and presence of pollutants in 90% water/DMF solution. (a, b) TPE-TPE, (c, d) TPE-TPE-CN. Concentration: 20 μmol/L. Excitation wavelength: TPE-TPE 310 nm, TPE-TPE-CN 365 nm. Data are presented as mean ± SD ($n = 3$).

and average diameter of these two types of organic nanoparticles show little change after 48 h (191.8 nm for TPE-TPE and 209.5 nm for TPE-TPE-CN, respectively), demonstrating good long-term stability of sulfates-based nanoparticles (Fig. S3 in Supporting information). All of the above demonstrates the typical AIE characteristic of these two TPE-based derivatives both in their solid and aggregated state.

To study the fluorescent detection property of these two TPE-based probes, their PL spectrum towards ROX with different concentrations in 90% water/DMF solution are studied, respectively. As shown in Figs. 2a and c, TPE-TPE and TPE-TPE-CN exhibit strong blue light and green light emission in the absence of ROX, respectively. But with the addition of ROX, the PL intensity of TPE-TPE at 471 nm gradually decreased, and finally decreased to 13.69-fold its original state with a very weak blue light emission in the presence of 1800 μmol/L of ROX. Similarly, the PL intensity of TPE-TPE-CN at 514 nm gradually reduced and reduced to 9.36-fold its original state with a very weak green light emission in the presence of 1800 μmol/L of ROX, which can be attributed to the PET effect between the ROX and the fluorescent probes [49,50]. Moreover, as shown in Figs. 2b and d, the value of $(P_0 - P)/P$ at λ_{em} was gradually increased with the concentration increase of ROX, and a good linear relationship between the PL intensity of the probes and the concentration of ROX (0–800 μmol/L) can be observed ($R^2 = 0.9922$ for TPE-TPE, $R^2 = 0.9530$ for TPE-TPE-CN), respectively. According to the $3\sigma/m$ method (where the σ represents the standard derivation standard deviation of the value of the fluorescence probes in 10 blank fluorescence measurements, and the m represents the slope of the titration curves of the probes), the detection limit of TPE-TPE and TPE-TPE-CN can be finally calculated as 0.154 and 0.385 μmol/L, respectively, which are below the safety concentration of ROX formulated by the World Health Organization (WHO) (1.90 μmol/L) and some works (Tables S2 and S3 in Supporting information) [10,15,17,51], demonstrating a good potential of our probes for organic arsenic detection in water.

It should be noted that there are many other pollutants including inorganic cationic and anionic ions and organics can be found in water. Therefore, fourteen types of pollutants including Na^+, NH_4^+, Ca^{2+}, Mg^{2+}, Cl^-, SO_4^{2-}, PO_4^{3-}, erythromycin (ERY), thiamphenicol (THI), *p*-arsanilic acid (ASA), *p*-hydroxyphenylarsonic acid (HAA), phenylamine (PLE), glycine (GLN) and L-aspartic acid (ARE) are introduced to study the selectivity of the fluorescent probes towards ROX, respectively. Interestingly, compared with the blank sample, the PL intensity of TPE-TPE and TPE-TPE-CN show an obvious decrease in the presence of 600 μmol/L of ROX, while changed a little in the presence of other cationic/anionic ions and organics (Figs. 3a and c). Moreover, their PL intensities at λ_{em} show a little decrease in the absence of ROX but decrease about 1.44–2.42-fold and 0.87–1.51-fold in the presence of ROX (Figs. 3b and d). Additionally, it is worth noting that Na^+ and Cl^- are widely distributed in water, and it is of significance to study their effect on detection [52]. To study the influence of Na^+ and Cl^-, the PL spectra of the probes in the presence of NaCl with different concentrations (0.6, 10, and 100 mmol/L) were measured, respectively. As shown in Fig. S4 (Supporting information), with the concentration increase of NaCl (from 0.6 mmol/L to 100 mmol/L), their PL spectra and PL intensity at λ_{em} show little decrease in the absence of ROX (0.07–0.23-fold for TPE-TPE, and 0.07–0.06-fold for TPE-TPE-CN), but decrease about 1.29–2.20-fold and 1.29–1.32-fold in the presence of ROX, demonstrating that Na^+ and Cl^- have negligible effect on detection performance of the probes. All of the above suggests that these two probes exhibit superior selectivity and anti-interference behaviors toward ROX in water.

It is known to all that PET is a typical fluorescent quenching mechanism in fluorescent detection. If the lowest unoccupied molecular orbital (LUMO) energy of a fluorescence probe is higher than that of the pollutant, the excited electrons will transfer from the fluorescence probe to the pollutant, leading to fluorescence quenching. Therefore, to explain the superior selectivity of TPE-TPE and TPE-TPE-CN towards ROX in water, their energies of highest occupied molecular orbital (HOMO) and LUMO were obtained *via* a density functional theory (DFT) calculation in Materials Studio (DMol3) (Fig. 4a and Fig. S5 in Supporting information). According to Fig. 4b, the LUMO energies of TPE-TPE and TPE-TPE-CN are −2.511 and −3.218 eV, respectively. For pollutants, the LUMO

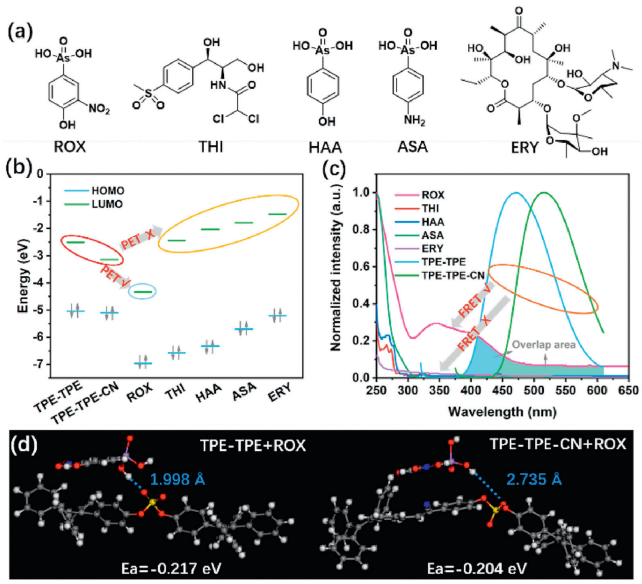

Fig. 4. The possible detection mechanism of TPE-TPE and TPE-TPE-CN for organic arsenic. (a) Structure of pollutants. (b) HOMO and LUMO energies of TPE-TPE, TPE-TPE-CN, and pollutants obtained by DFT calculation. (c) Overlap of adsorption spectra of pollutants and PL spectra of the probes in 90% water/DMF. (d) Adsorption energy of the probes-ROX system from DFT calculation, from left to right: TPE-TPE+ROX and TPE-TPE-CN+ROX. The white, gray, red, purple, and blue balls represent hydrogen, carbon, oxygen, arsenic, and nitrogen atoms, respectively. Concentration: 20 μmol/L. Excitation wavelength: TPE-TPE 310 nm, TPE-TPE-CN 365 nm.

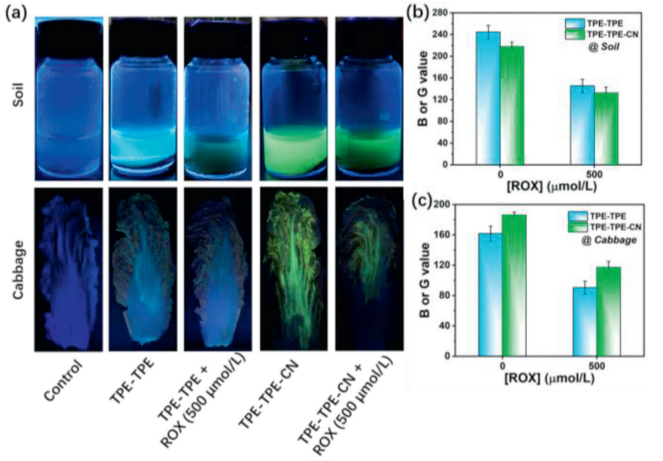

Fig. 5. Applications of the probes for ROX detection in soil and cabbage. (a) Fluorescent photos and (b, c) corresponding B or G value changes obtained in a color discriminator of TPE-TPE and TPE-TPE-CN in the absence and presence of ROX (500 μmol/L) in 90% water/DMF solution (top) and cabbage (bottom). Concentration of the probes: 10 μmol/L. Data are presented as mean ± SD ($n = 3$).

energy of ROX is −4.338 eV, which is much lower than that of other pollutants such as THI (−2.445 eV), HAA (−2.037 eV), ASA (−1.789 eV) and ERY (−1.472 eV). Moreover, the LUMO energies of the probes are higher than that of ROX, but lower than that of other pollutants, indicating that the excited electron transfer from the probes to ROX is more thermodynamically-favored than that of other pollutants. Interestingly, the LUMO energy gap between TPE-TPE and ROX is higher than that between TPE-TPE-CN and ROX, suggesting that electron transfer of TPE-TPE at excited state is more likely to be absorbed by ROX, and resulting in greater attenuation in fluorescence.

Additionally, FRET is another fluorescent quenching mechanism during fluorescent detection [53,54]. In the FRET process, a whole/partial overlap between the PL spectrum of a fluorescent probe (FRET donor) and the absorbance spectrum of a pollutant (FRET acceptor) will give rise to fluorescent quenching of the fluorescent probe. Therefore, the UV–vis adsorption spectra of these pollutants and the PL spectra of the probes are measured, respectively. As shown in Fig. 4c, an obvious overlap between the PL spectra of the probes and the absorbance of ROX can be observed, which means that energy can be transferred from the excited-state probes (FRET donor) to ROX (FRET acceptor), giving rise to fluorescent quenching of TPE-TPE (-CN). However, the FRET effect would be ignorable for other pollutants due to the deficiency of overlap between their absorption spectra and the PL spectra of the probes, indicating that the FRET effect contributed partially to fluorescent quenching during detection. Furthermore, the degree of overlap between the PL spectra of TPE-TPE and the absorption spectra of ROX is higher than that between TPE-TPE-CN and ROX, resulting in more striking attenuation of fluorescence for TPE-TPE after detection. Moreover, since fluorescent quenching can be regarded as a result of molecular interaction between the probe and ROX, the adsorption energies of the probes towards ROX were obtained *via* a DFT calculation method. According to Fig. 4d, a hydrogen bond between the hydroxyl group of ROX and the oxygen atom of the sulfate group can be obtained under optimal structure, and the length of the hydrogen bond in the TPE-TPE+ROX system is 0.1998 nm, which is shorter than that of the TPE-TPE-CN+ROX system (0.2375 nm). Moreover, the adsorption energy (E_a) of the TPE-TPE+ROX system is −0.217 eV, which is lower than that of the TPE-TPE-CN+ROX system (−0.204 eV), indicating that the pollutant is more inclined to be adsorbed on the surface of TPE-TPE during detection. In a word, a higher LUMO energy gap, greater spectra overlap area and stronger interaction between TPE-TPE and ROX endow it with a high sensitivity and low detection limit towards ROX.

To study the practical application of these two AIE probes for ROX detection in real water samples (including tap water, bottled water, and lake water), the fluorescent responses of TPE-TPE and TPE-TPE-CN towards 100 and 400 μmol/L of ROX were studied, respectively. As shown in Table 1, the recovery rates of the real water samples were in the range of 95%–105% with acceptable relative standard deviations (RSD, 3.14%–11.03%), demonstrating that these two probes can be used to detect ROX in the real water samples. Moreover, a real-time scanometric monitoring method just using a smartphone was also conducted at room temperature to explore the practical application of these two probes. According to Fig. S6a (Supporting information), the blue light emission of TPE-TPE and green light emission of TPE-TPE-CN depressed with the concentration increase of ROX under UV light at 365 nm. Accordingly, with the concentration increase of ROX, the B value of TPE-TPE and G value of TPE-TPE-CN are gradually decreased, respectively. Moreover, a good linear relationship between the concentration of ROX (0–1000 μmol/L) and the B or G value of the probes can also be obtained ($R^2 = 0.9914$ and 0.9939), respectively, indicating that our fluorescent probes can be potentially used as a real-time detector in practical application with high accuracy and efficiency (Figs. S6b and c in Supporting information). In addition, in terms of the above results, TPE-TPE and TPE-TPE-CN are used to detect ROX in soil and cabbage to explore their multivariate application. As shown in Fig. 5a, the probe solution (water/DMF = 9/1, v/v) displays strong blue and green emission in the absence of ROX, but very weak emission in the presence of 500 μmol/L of ROX. A similar fluorescent quenching phenomenon can also be observed on the surface of cabbage, resulting from the PET and FRET effect between the probes and ROX at an excited state. Furthermore, with the aid of a smartphone and portable UV light, the B and G value change of these two probes before and after detection can be obtained (Figs. 5b and c). For soil detection, the B value of TPE-TPE and G value of

Table 1
Applications of TPE-TPE and TPE-TPE-CN for ROX detection in real water samples.[a]

Probes and pollutants	ROX	Tap water		Bottled water		Lake water	
	Spiked (μmol/L)	Recovery (%)	RSD (%, $n=3$)	Recovery (%)	RSD (%, $n=3$)	Recovery (%)	RSD (%, $n=3$)
TPE-TPE	0	-[b]	-	-	-	–	–
	100	97.86	6.84	99.54	5.81	100.66	11.03
	400	95.88	5.44	102.82	3.26	95.18	7.23
TPE-TPE-CN	0	-	-	-	-[b]	–	–
	100	100.06	7.36	103.54	6.98	98.35	3.14
	400	98.73	5.69	95.00	7.91	96.23	6.54

[a] Concentration of the probes: 20 μmol/L.
[b] Not detected.

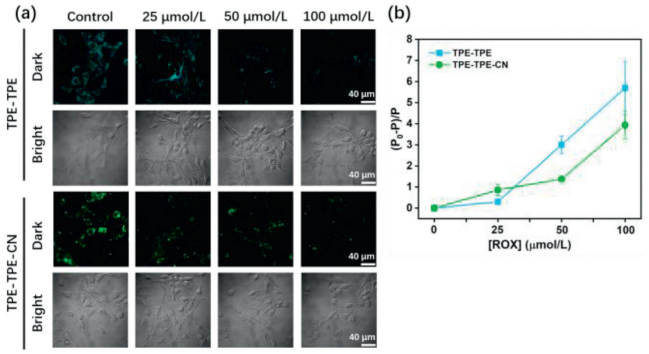

Fig. 6. Application of TPE-TPE and TPE-TPE-CN for ROX detection in living cells. (a) Confocal fluorescent images of TPE-TPE and TPE-TPE-CN (from top to bottom) in the absence and presence of ROX with different concentrations (control, 25–100 μmol/L, from left to right) in living 3T3 cells. (b) PL intensity changes of TPE-TPE and TPE-TPE-CN in the presence of different ROX in living 3T3 cells. P_0 and P are PL intensity at λ_{em} of the probes in the absence and presence of ROX in 3T3 cells. The concentration of the probes: 10 μmol/L, excitation wavelength: 404 nm. Scale bar: 40 μm. Data are presented as mean ± SD ($n=3$).

TPE-TPE-CN decreased 1.682-fold and 1.645-fold, respectively. And for cabbage detection, their corresponding reduction is 1.79-fold and 1.59-fold, respectively. All above indicates that our AIE probes exhibit wide application potential for ROX detection in water, soil, and even in food samples.

Besides, these two probes are also used to detect ROX in living 3T3 cells to explore their potential application in organisms. According to Fig. S7 (Supporting information), compared with the control groups, all the 3T3 cells display equivalent viability in the presence of TPE-TPE, TPE-TPE-CN, and ROX with concentrations from 1 μmol/L to 100 μmol/L, suggesting superior non-toxicity of the fluorescence probes. Herein, in consideration of the aggregation state of these two fluorescent nanoparticles, the concentration of the probes is 10 μmol/L. Moreover, to obtain optimal cellular uptake time, 3T3 cells were incubated with the two probes with different uptake times ranging from 1 h to 24 h. As shown in Fig. S8 (Supporting information), with the increase of incubation time (0–8 h), the fluorescent probes are gradually swollen by the cells and exhibit bright light emission. But when the duration is longer than 8 h, the gradual aggregation of fluorescent nanoparticles constrains the uptake capacity of the cells, attributing to the formed large particles of probes that cannot be easily swollen by the cells. Therefore, the 3T3 cells were incubated optimally with fluorescent nanoparticles for 8 h. Furthermore, the feeding 3T3 cells were incubated with ROX in with concentration ranging from 25 μmol/L to 100 μmol/L for another 8 h to study their detection property in living cells. As shown in Fig. 6a, the cells display bright blue and green light emissions in the absence of ROX, respectively. With the concentration increase of ROX, the bright blue and green light emission were gradually depressed and almost quenched in the presence of 100 μmol/L of ROX, which were consistent with their corresponding changes in PL intensity. According to Fig. 6b, the PL intensity of TPE-TPE and TPE-TPE-CN gradually decreased with the increase of ROX, and even decreased by 5.69-fold and 3.94-fold in 100 μmol/L of ROX, respectively. Notably, the degree of decrease in PL intensity of TPE-TPE was greater than that of TPE-TPE-CN at a higher concentration of ROX (100 μmol/L), indicating a good sensitivity of TPE-TPE towards ROX in living cells, which is consistent with their results for ROX detection in water. In a word, all the above demonstrated an excellent application potential of our AIE probes for ROX detection not only in real environments (including water, soil, and food) but also in living cells.

In summary, two TPE-based derivatives with typical AIE characteristics both in their solid and aggregated state were successfully fabricated *via* the SuFEx reaction. These two fluorescent probes can be used to selectively detect low concentrations of organic arsenic in water on account of the PET and FRET effect between the probes and pollutants. Moreover, these two probes exhibit superior detection performance for organic arsenic both in real environments and living cells. Our study provides a new strategy for the development of AIE-active probes for monitoring organic pollutants with low concentrations in the environment and living cells.

Declaration of competing interest

The authors declare that they have no known competing financial interests or personal relationships that could have appeared to influence the work reported in this paper.

CRediT authorship contribution statement

Haibo Wan: Writing – review & editing, Writing – original draft, Data curation. **Zhengzhong Lv:** Data curation. **Jicai Jiang:** Formal analysis. **Xuefeng Cheng:** Software. **Qingfeng Xu:** Supervision, Funding acquisition. **Haibin Shi:** Supervision. **Jianmei Lu:** Writing – review & editing, Supervision, Funding acquisition.

Acknowledgments

We acknowledge financial support from the National Natural Science Foundation of China (Nos. 21938006, 21776190), Basic Research Project of Leading Technology (No. BK20202012), the Natural Science Foundation of the Jiangsu Higher Education Institutions of China (No. 20KJA610001), PAPD in Jiangsu Province, China Postdoctoral Science Foundation (No. 2022M722308), and Jiangsu Province Excellent Postdoctoral Program (No. 2022ZB563). We also extend our gratitude to Huan Luo from Shiyanjia Lab (www.shiyanjia.com) for providing invaluable assistance with the fluorescence analysis.

Supplementary materials

Supplementary material associated with this article can be found, in the online version, at doi:10.1016/j.cclet.2024.110023.

References

[1] M. Wen, Y. Liu, Q. Zhang, et al., Chemosphere 311 (2023) 137118.
[2] J. Ma, Y. Wu, C. Xu, et al., J. Hazard. Mater. 454 (2023) 131483.
[3] S. Balu, Y.L. Chen, S.W. Chen, T.C.K. Yang, Appl. Catal. B: Environ. 304 (2022) 120852.
[4] S. Gong, J. Yang, Q. Pan, et al., Water Res. 237 (2023) 119979.
[5] D. Zhao, J. Wang, D. Yin, et al., J. Hazard. Mater. 383 (2020) 121178.
[6] L. Shi, W. Wang, S. Yuan, Z. Hu, Environ. Sci. Technol. 48 (2014) 7951–7958.
[7] K. Huang, H. Peng, F. Gao, et al., Environ. Pollut. 247 (2019) 482–487.
[8] H. Zhong, B. Zhao, J. Deng, Small 19 (2023) 2300961.
[9] Y. Yang, X. Liu, S. Meng, et al., J. Hazard. Mater. 458 (2023) 131941.
[10] H. Chen, W. Liu, L. Cheng, et al., Chem. Eng. J. 429 (2022) 132162.
[11] K. Zhu, J. Wu, R. Fan, et al., Chem. Eng. J. 427 (2022) 131483.
[12] N. Seal, A.S. Palakkal, R.S. Pillai, S. Neogi, Inorg. Chem. 62 (2023) 11528–11540.
[13] G.K. Dam, S. Fajal, S. Dutta, et al., ACS Appl. Opt. Mater. 1 (2023) 1217–1226.
[14] J. Lv, B. Wang, Y. Xie, et al., Environ. Sci. Nano 6 (2019) 2759–2766.
[15] Z. Li, H. Zhang, T. He, et al., Inorg. Chim. Acta 547 (2023) 121334.
[16] D.B. Kanzariya, T.S. Khan, S. Das, et al., Dalton Trans. 51 (2022) 7436–7454.
[17] C. Wang, G. Ren, Q. Tan, et al., Spectrochim. Acta. A: Mol. Biomol. Spectrosc. 299 (2023) 122812.
[18] F. Li, J. Gao, H. Wu, et al., Nanomaterials 12 (2022) 2997.
[19] A. Mishra, P. Bäuerle, Angew. Chem. Int. Ed. 51 (2012) 2020–2067.
[20] Y. Liang, C. Xu, H. Zhang, et al., Angew. Chem. Int. Ed. 62 (2023) e202217616.
[21] J. Mei, N.L. Leung, R.T. Kwok, J.W. Lam, B.Z. Tang, Chem. Rev. 115 (2015) 11718–11940.
[22] W. Qiao, T. Ma, S. Wang, et al., Adv. Funct. Mater. 31 (2021) 2105452.
[23] X. Yang, C. Xu, X. Zhang, et al., Adv. Funct. Mater. 33 (2023) 2300746.
[24] H. Wan, Q. Xu, P. Gu, et al., J. Hazard. Mater. 403 (2021) 123656.
[25] Y. Liu, X. Chen, X. Liu, W. Guan, C. Lu, Chem. Soc. Rev. 52 (2023) 1456–1490.
[26] C. Xu, Y. Zhou, Z. Li, et al., J. Hazard. Mater. 418 (2021) 126243.
[27] J. Qin, X. Li, W. Lang, F. Zhang, Q. Cao, Chin. Chem. Lett. 35 (2023) 108925.
[28] Y. Pan, Y. Guo, Y. Li, L. Tang, X. Yan, Chin. Chem. Lett. 34 (2023) 108237.
[29] J. Zhao, W. Xu, B. Li, et al., Chin. Chem. Lett. 35 (2024) 108579.
[30] P. Chen, P. Lv, C. Guo, et al., Chin. Chem. Lett. 34 (2023) 108041.
[31] X. Cheng, S. Huang, Q. Lei, et al., Chin. Chem. Lett. 33 (2022) 1861–1864.
[32] M.C. Claire, Y. Hong, Aggregate 4 (2023) e336.
[33] F. Sun, S. Tan, H. Cao, et al., Angew. Chem. Int. Ed. 134 (2022) e202207125.
[34] F. Hu, G. Qi, Kenry, D. Mao, et al., Angew. Chem. Int. Ed. 59 (2020) 9288–9292.
[35] A. Barrow, C. Smedley, Q. Zheng, et al., Chem. Soc. Rev. 48 (2019) 4731–4758.
[36] J. Dong, L. Krasnova, M. Finn, K.B. Sharpless, Angew. Chem. Int. Ed. 53 (2014) 9430–9448.
[37] S. Li, G. Li, B. Gao, et al., Nat. Chem. 13 (2021) 858–867.
[38] H. Kim, J. Zhao, J. Bae, et al., ACS Cent. Sci. 7 (2021) 1919–1928.
[39] H. Wan, Q. Xu, J. Wu, et al., Angew. Chem. Int. Ed. 134 (2022) e202208577.
[40] H. Zhu, D. Chen, N. Li, et al., Chem. Eur. J. 23 (2017) 14712–14717.
[41] X. Xiao, F. Zhou, J. Jiang, et al., Polym. Chem. 9 (2018) 1040–1044.
[42] C. Xia, C. Liu, F. Zhou, et al., Chem. Asian J. 14 (2019) 4296–4302.
[43] H. Li, B.S. Chang, H. Kim, et al., Joule 7 (2023) 95–111.
[44] H. Wan, S. Zhou, P. Gu, et al., Polym. Chem. 11 (2020) 1033–1042.
[45] J. Wu, H. Wan, S. Zhou, et al., Chem. Asian J. 16 (2021) 3202–3208.
[46] S. Kitamura, Q. Zheng, J.L. Woehl, et al., J. Am. Chem. Soc. 142 (2020) 10899–10904.
[47] Q. Zheng, J.L. Woehl, S. Kitamura, et al., Proc. Natl. Acad. Sci. U. S. A. 116 (2019) 18808–18814.
[48] Y. Ding, Z. Tong, L. Jin, et al., Adv. Mater. 34 (2022) 2106388.
[49] J.D. Jensen, R.K. Jakobsen, Z. Yao, B.W. Laursen, Chem. Eur. J. 29 (2023) e202301077.
[50] J. Bai, J. Wang, H. Zheng, et al., Small 19 (2023) 2305024.
[51] J. Liu, H. Yu, H. Song, et al., J. Environ. Monitor. 10 (2008) 975–978.
[52] Y. Wu, Y. Xu, Y. Zhang, et al., Chin. Chem. Lett. 33 (2022) 2741–2746.
[53] D. Wang, L. Zhang, M. Liu, et al., J. Hazard. Mater. 454 (2023) 131497.
[54] D.S. Biswas, P. Gaki, E.C.D. Silva, et al., Adv. Mater. 35 (2023) 2301402.